nature chemical biology

ARTICLE

PUBLISHED ONLINE: 30 MARCH 2015 | DOI: 10.1038/NCHEMBIO.1788

Impeding the interaction between Nur77 and p38 reduces LPS-induced inflammation

Li Li[1,3], Yuan Liu[1,3], Hang-zi Chen[1,3], Feng-wei Li[1,3], Jian-feng Wu[1], Hong-kui Zhang[2], Jian-ping He[1], Yong-zhen Xing[1], Yan Chen[1], Wei-jia Wang[1], Xu-yang Tian[1], An-zhong Li[1], Qian Zhang[1], Pei-qiang Huang[2], Jiahuai Han[1], Tianwei Lin[1]* & Qiao Wu[1]*

Sepsis, a hyperinflammatory response that can result in multiple organ dysfunctions, is a leading cause of mortality from infection. Here, we show that orphan nuclear receptor Nur77 (also known as TR3) can enhance resistance to lipopolysaccharide (LPS)-induced sepsis in mice by inhibiting NF-κB activity and suppressing aberrant cytokine production. Nur77 directly associates with p65 to block its binding to the κB element. However, this function of Nur77 is countered by the LPS-activated p38α phosphorylation of Nur77. Dampening the interaction between Nur77 and p38α would favor Nur77 suppression of the hyperinflammatory response. A compound, *n*-pentyl 2-[3,5-dihydroxy-2-(1-nonanoyl) phenyl]acetate, screened from a Nur77-biased library, blocked the Nur77-p38α interaction by targeting the ligand-binding domain of Nur77 and restored the suppression of the hyperinflammatory response through Nur77 inhibition of NF-κB. This study associates the nuclear receptor with immune homeostasis and implicates a new therapeutic strategy to treat hyperinflammatory responses by targeting a p38α substrate to modulate p38α-regulated functions.

Sepsis is an uncontrolled systemic inflammation from an infection. Severe sepsis may result in organ failure and even death. In the early phase of septic shock, proinflammatory cytokines have a crucial role in activating lymphocytes, phagocytes and vascular endothelium and in stimulating the release of secondary mediators to increase vascular permeability, which causes tissue damage[1,2]. The uncontrolled production of proinflammatory cytokines can be more damaging than the primary infection[3], and to prevent septic shock, it is of great importance to terminate the excess production of proinflammatory cytokines.

LPS (also called endotoxin) from the outer membrane of Gram-negative bacteria incites life-threatening endotoxic shock[4]. It can rapidly activate mitogen-activated protein kinases (MAPKs, including ERK, JNK and p38), IκB kinases (IKKs) and several downstream transcription factors to control the expression of proinflammatory cytokines[5,6]. Among these transcription factors, NF-κB has a central role. NF-κB comprises two subunits, p65 and p50, which are retained in the cytoplasm by the inhibitory IκBs. Upon stimulation, IκBs are phosphorylated by IKKs and degraded through the ubiquitin-proteasome pathway, leading to the translocation of transcription-competent NF-κB to the nucleus[7].

MAPK p38 has been implicated as a critical factor upstream of NF-κB[8,9]. It upregulates the expression of a variety of genes in the acute phase of inflammatory responses[10]. Blocking p38 with specific inhibitors attenuates the expression of NF-κB target genes. However, the nuclear translocation or DNA-binding activity of NF-κB does not seem contingent on p38 activity[8], which suggests that p38's influence on NF-κB may be indirect. It is reported that, upon stimulation by a combination of interleukin-1β (IL-1β) and interferon-γ (IFN-γ), p38 phosphorylates acetyltransferase coactivator p300 to enhance its association with and its acetylation of p65 to activate NF-κB activity in primary human astrocytes[11]. Still, many unknown factors in the p38-dependent regulation of NF-κB await further investigation.

Orphan nuclear receptor Nur77 (also called TR3) belongs to the NR4A family of nuclear receptors[12]. Nur77 expression can be rapidly induced by a variety of inflammatory stimuli through NF-κB binding to the Nur77 promoter in monocytes and macrophages[13]. The anti-inflammatory property of Nur77 has been demonstrated in various cell models. Elevation of Nur77 expression reduced the expression of several cytokines and chemokines in macrophages in response to LPS or TNF-α stimulation[14]. Nur77 suppressed monocyte adhesion by upregulating IκBα expression in human endothelial cells[15]. Mice deficient in Nur77 showed enhanced atherosclerosis and chronic inflammatory disease owing to impaired Toll-like receptor signaling as well as macrophages polarized toward an inflammatory phenotype[16,17]. Yet the applicability of Nur77 as a molecular target in inflammatory diseases is still to be substantiated.

This study reports a mechanism in which NF-κB activity is downregulated through a direct Nur77 interaction with p65 to block its binding to the κB element. This Nur77 inhibition, however, is abruptly countered by p38α phosphorylation. Interference with the associated p38α-Nur77 interaction would favor Nur77's attenuation of the LPS-induced hyperinflammatory response. To this end, a chemical compound, *n*-pentyl 2-[3,5-dihydroxy -2-(1-nonanoyl)-phenyl]acetate (PDNPA), which targets the ligand-binding domain (LBD) of Nur77, was identified from an in-house, Nur77-biased library. By impeding the interaction between Nur77 and p38α, PDNPA abolishes the p38α phosphorylation of Nur77 so that Nur77 can effectively inhibit NF-κB activity and, as a result, dampen LPS-induced inflammation.

RESULTS

Nur77 knockout makes mice more susceptible to sepsis

To define the role of Nur77 in sepsis, we used LPS to induce the initial phase of sepsis in wild-type (WT) mice and Nur77 knockout (KO) mice. Although both displayed the symptoms of endotoxic

[1]State Key Laboratory of Cellular Stress Biology, Innovation Center for Cell Signaling Network, State-Province Joint Engineering Laboratory of Targeted Drugs from Natural Products, School of Life Sciences, Xiamen University, Xiamen, Fujian Province, China. [2]Key Laboratory for Chemical Biology of Fujian Province, College of Chemistry and Chemical Engineering, Xiamen University, Xiamen, Fujian Province, China. [3]These authors contributed equally to this work. *e-mail: twlin@xmu.edu.cn or qiaow@xmu.edu.cn

shock under LPS treatment, such as crouching, shivering and disheveled fur, the mortality rate of KO mice was evidently increased (**Fig. 1a**). The body temperature of KO mice also dropped faster in the first 24 h of the LPS injection (**Fig. 1a**). These results suggest that Nur77-deficient mice are more susceptible to LPS challenge.

To assess Nur77's role in organ failure in sepsis, the blood urea nitrogen (BUN) level and renal histology were monitored for kidney function. The BUN level increased modestly in WT mice but was approximately three times above the background level in KO mice after LPS injection (**Supplementary Results**, **Supplementary Fig. 1a**). Accumulation of red blood cells and tubule dilation were also more evident in the kidneys of KO mice after LPS administration (**Supplementary Fig. 1b**). These results indicate renal dysfunction in Nur77-deficient mice upon LPS challenge.

LPS-induced endotoxic shock is accompanied by increased production of proinflammatory cytokines. After LPS administration, serum concentrations of TNF-α and IL-6 in KO mice were initially approximately two- to threefold higher than those in WT mice but then dropped to comparable levels in 8 h. The IL-1β concentration in KO mice was elevated to a much higher level than in WT mice for a duration of 8 h. The nitric oxide (NO) content, an important inflammatory mediator, was also obviously higher in KO than in WT mice in the first 6 h of LPS injection (**Fig. 1b**). These results indicate that Nur77-deficient mice are more susceptible to endotoxic shock, probably owing to the presence of excess cytokines and inflammatory mediators.

The cecal ligation and puncture (CLP) mouse model was also used for the investigation. CLP induces a polymicrobial sepsis that mimics the later phase of human sepsis[18]. All KO mice died within 3 d after CLP, whereas over 20% of WT mice survived by day 7 (**Supplementary Fig. 1c**). In contrast to WT mice, KO mice had much higher levels of bacteria in both spleen and blood (**Supplementary Fig. 1d**,**e**) as well as more severe kidney injury (**Supplementary Fig. 1f**,**g**), indicating that they lost the capacity to clear blood-borne bacteria. The levels of proinflammatory cytokines, including TNF-α, IL-6 and IL-1β, were also two- to threefold higher in KO mice than in WT mice after CLP (**Supplementary Fig. 1h**). These data suggest that the major role for Nur77 is also to limit the production of proinflammatory cytokines in the later phase of sepsis.

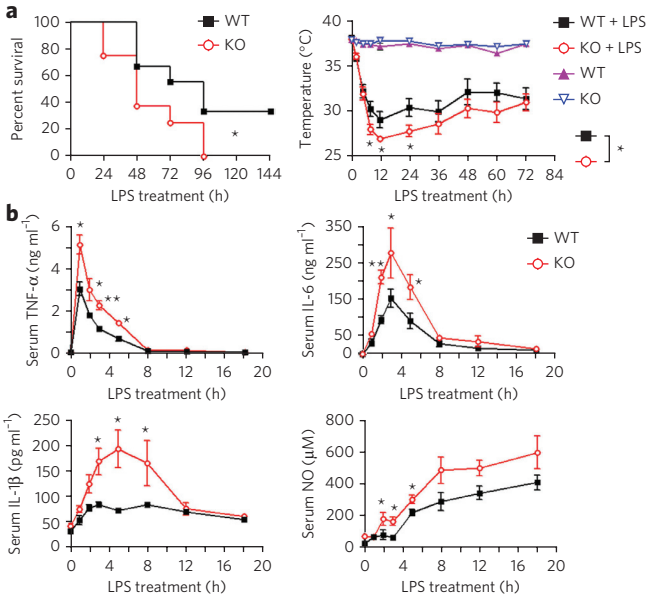

Figure 1 | Nur77-deficient mice are with elevated sensitivity to LPS-induced sepsis. (**a**) Nur77-deficient mice are more vulnerable to LPS-induced death. WT and KO mice were intraperitoneally injected with LPS (10 mg per kg body weight; $n = 15$). Survival rates (left) and body temperatures (right) were recorded. (**b**) Release of serum inflammatory mediators in WT and KO mice. After LPS injection, sera from mice ($n = 6$) were collected at the indicated times for analysis of TNF-α, IL-6 and IL-1β by ELISA and of NO by bioassay. Kaplan-Meier plots were made, and statistical significance was analyzed by a log-rank test. Differences between the two groups are assessed by two-way ANOVA using SPSS software. Representatives of three independent experiments with similar results are shown. $^{*}P < 0.05$, $^{**}P < 0.01$.

Nur77 blocks p65 binding to DNA

Peritoneal macrophages were isolated from WT and KO mice (*Nr4a1*$^{+/+}$ and *Nr4a1*$^{-/-}$ macrophages, henceforth referred to as *Nur77*$^{+/+}$ and *Nur77*$^{-/-}$ macrophages, respectively) for the investigation. After LPS stimulation, the concentrations of TNF-α, IL-6, IL-1β and NO were much higher in the culture medium of *Nur77*$^{-/-}$ than *Nur77*$^{+/+}$ macrophages (**Supplementary Fig. 2a**), another indication that Nur77 downregulates the production of proinflammatory cytokines. To evaluate Nur77's influence on the LPS-induced pathways on a global scale, microarrays were used to assay gene expression in LPS-stimulated *Nur77*$^{+/+}$ and *Nur77*$^{-/-}$ macrophages. Most of the LPS-inducible genes[19] were expressed at much higher levels in *Nur77*$^{-/-}$ macrophages (**Supplementary Fig. 2b**). In addition, *Nur77*$^{-/-}$ macrophages expressed more NF-κB–dependent genes[20] than did *Nur77*$^{+/+}$ macrophages upon LPS stimulation (**Supplementary Fig. 2c** and **Supplementary Table 1**). Gene set enrichment analysis (GSEA) also implied that LPS-downregulated[19,21] or NF-κB–inhibited[20,22] gene signatures were markedly enriched, whereas LPS- or NF-κB–upregulated gene signatures were negatively enriched in *Nur77*$^{+/+}$ macrophages (**Supplementary Fig. 2d**). These results lend support to the notion that Nur77 is a negative regulator in the LPS-stimulated inflammatory response and is negatively correlated with the NF-κB downstream targets.

IκB is a negative regulator of NF-κB[23]. Although overexpression of Nur77 increased IκB-α expression, which suppressed NF-κB activation in endothelial cells[15], there is no difference in IκB-α expression between *Nur77*$^{+/+}$ and *Nur77*$^{-/-}$ macrophages with or without the LPS induction (**Supplementary Fig. 2e**). Moreover, p65 had comparable levels of expression and nuclear translocation in both *Nur77*$^{+/+}$ and *Nur77*$^{-/-}$ macrophages before and after LPS treatment (**Supplementary Fig. 2e**). It is possible that Nur77 directly influences the transcription activity of NF-κB in macrophages. Indeed, transfection of p65 greatly activated NF-κB reporter activity in 293T cells, which could be significantly inhibited by Nur77 (**Fig. 2a**). LPS-induced NF-κB reporter activity in RAW264.7 macrophages was further enhanced by transfecting Nur77-targeted siRNA (**Fig. 2a**), indicating that Nur77 attenuates LPS-induced NF-κB activity.

Nur77's influence on p65 binding to DNA was investigated by an electrophoretic mobility shift assay (EMSA) with a specific NF-κB probe. In *Nur77*$^{+/+}$ macrophages, DNA interaction with p65 was observed after LPS induction, which was gradually weakened afterwards. In contrast, p65 binding to DNA was increased with the addition of LPS in *Nur77*$^{-/-}$ macrophages for as long as 8 h (**Fig. 2b**). This Nur77 modulation of NF-κB DNA binding activity was also demonstrated by an *in vitro* assay, in which p65 binding to its response element was suppressed by recombinant Nur77 (**Supplementary Fig. 2f**). This suppression might originate from a direct contact, as Nur77 and p65 showed interaction in both co-immunoprecipitation (co-IP) and glutathione S-transferase (GST) pulldown assays (**Supplementary Fig. 2g**) involving both the transactivation domain (TAD) of Nur77 and the LBD (**Supplementary Fig. 2h**,**i**). The interaction between the LBD and p65 was reported previously[24]. However, transfection of the TAD alone, but not the LBD alone, was sufficient to suppress NF-κB reporter activity

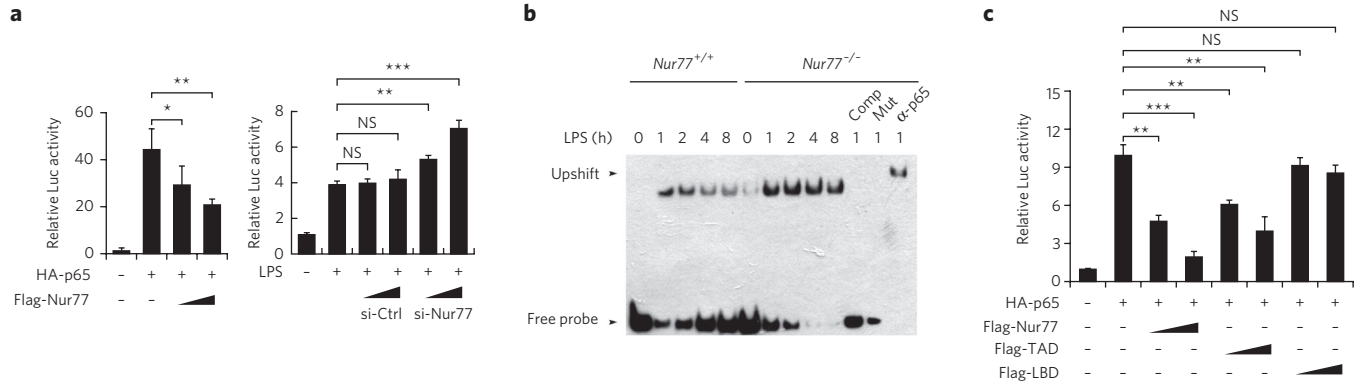

Figure 2 | Nur77 inhibits NF-κB activation via impairing p65 binding to DNA. (**a**) Nur77 suppresses NF-κB transactivation activity. The NF-κB reporter gene, together with p65 and Nur77, was transfected into 293T cells (left). RAW264.7 cells were transfected with siRNA to Nur77 for 24 h, followed by LPS treatment for 9 h (right). The reporter activity was determined by luciferase (Luc) assays. HA, hemagglutinin. (**b**) Detection of p65 binding to DNA by EMSA using an NF-κB probe. *Nur77*$^{+/+}$ and *Nur77*$^{-/-}$ macrophages were treated with LPS for the times indicated. Anti-p65 antibody was preincubated with nuclear extracts to identify p65 (upshifted band). The same probe to NF-κB without biotin labeling was used as a competitor (Comp). Mutant probe to NF-κB (Mut) was used as a negative control. (**c**) Deletion of the TAD fails to suppress NF-κB activity. Plasmids were transfected into 293T cells as indicated, and the luciferase assay was performed. Images of full blots are shown in **Supplementary Figure 8**. Representatives of three independent experiments with similar results are shown. Results are presented as the mean ± s.e.m. **P* < 0.05, ***P* < 0.01, ****P* < 0.001. NS, no significance.

(**Fig. 2c**) and the LPS-induced expression of TNF-α mRNA (**Supplementary Fig. 2j**). Thus, Nur77 suppresses LPS-induced NF-κB activity by blocking p65 binding to DNA to attenuate the production of proinflammatory cytokines.

p38α phosphorylation hampers Nur77 inhibition of NF-κB

LPS activates a series of kinases, including MAPKs and IKKs, that target transcription factors to regulate the expressions of a large array of proinflammatory genes[5]. Nur77 is a phosphorylatable transcription factor, and the phosphorylation level of its threonine but not serine residues was evidently elevated upon LPS stimulation in RAW264.7 cells (**Fig. 3a**). In the same cell lysates, the activities of ERK, p38, JNK and IKK were all elevated by LPS (**Supplementary Fig. 3a**). However, only SB202190, an inhibitor to p38, inhibited the LPS-induced phosphorylation of Nur77 at threonine residues (**Fig. 3b**), suggesting that p38 is responsible for the LPS-induced phosphorylation of Nur77. The role of p38 in phosphorylating Nur77 was investigated by two additional approaches. First, cotransfection of p38α into 293T cells increased threonine phosphorylation in Nur77 (**Supplementary Fig. 3b**). Second, in macrophages isolated from LtrLys^{Cre}-p38α$^{Δ/Δ}$ mice, no phosphorylation of Nur77 was observed after LPS treatment. In contrast, LPS did induce threonine phosphorylation in Nur77 in p38α$^{fl/fl}$ macrophages with normal p38α expression (**Fig. 3c**). These results indicate that p38α selectively participates in LPS-induced phosphorylation of Nur77.

We also investigated the connection between p38α-induced phosphorylation of Nur77 and LPS-stimulated NF-κB activity. GST-Nur77 effectively blocked p65 binding to DNA, which was nullified by phosphorylated Nur77 from preincubation with a His-p38α (**Fig. 3d**). Furthermore, transfection of p38α, but not mutant p38α-AF, which had no kinase activity, reduced the interaction between Nur77 and p65 (**Supplementary Fig. 3c**). These findings

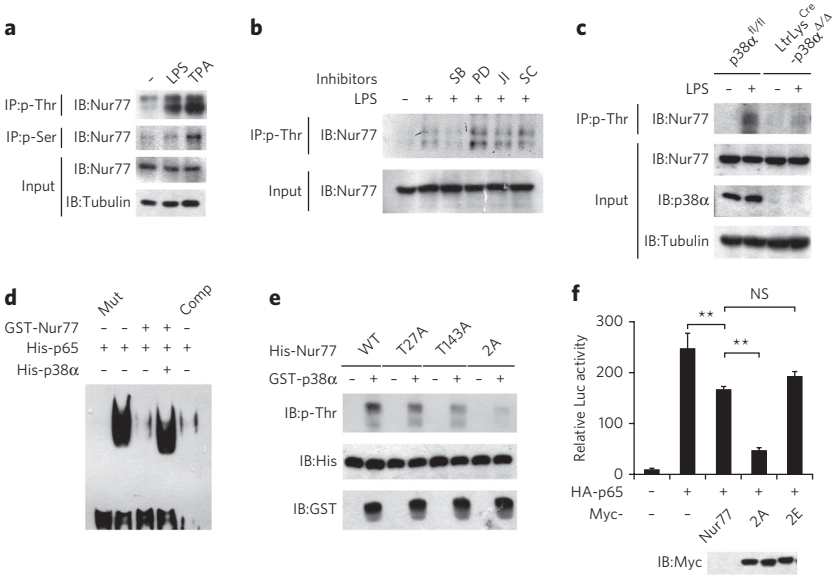

Figure 3 | Phosphorylation by p38α abolishes Nur77 function. (**a**) LPS induces phosphorylation in Nur77. RAW264.7 cells were treated with LPS (1 h). Phosphorylated Nur77 was immunoprecipitated (IP) with anti-phosphothreonine or anti-phosphoserine antibodies and analyzed with an anti-Nur77 antibody. TPA (100 ng ml^{-1}, 1 h) was used as a positive control. (**b**) Effect of kinase inhibitors on LPS-induced phosphorylation of Nur77. RAW264.7 cells were pretreated with different inhibitors (10 μM, 15 min) followed by LPS. Phosphorylated Nur77 was detected. SB, SB202190 for p38 inhibition; PD, PD98059 for ERK inhibition; JI, JNK inhibitor II; SC, SC-514 for IKK inhibition. (**c**) Effect of p38α on Nur77 phosphorylation. Macrophages separated from LtrLys^{Cre}-p38α$^{Δ/Δ}$ or p38$^{fl/fl}$ mice were treated with LPS. Phosphorylated Nur77 was detected. (**d**) p38α phosphorylation abolishes the Nur77 inhibition on p65 binding to DNA. GST-Nur77 was preincubated with His-p38α and subjected to EMSA. Mut, mutant probe; Comp, competitor. (**e**) p38α phosphorylates Nur77 at Thr27 and Thr143. Bacterially expressed GST-p38α was incubated with His-Nur77 or its mutants, and phosphorylated Nur77 was detected. IB, immunoblot. (**f**) Effect of Nur77 or its point mutants on NF-κB activity. Plasmids were transfected into 293T cells as indicated, and a luciferase assay was performed. Images of full blots are shown in **Supplementary Figure 8**. Results are presented as the mean ± s.e.m. Representatives of three independent experiments with similar results are shown. HA, hemagglutinin. ***P* < 0.01; NS, no significance.

imply that phosphorylation by p38α interferes with the interaction of Nur77 with p65, thereby abolishing Nur77's inhibition of p65 binding to DNA.

Co-IP showed that Nur77 interacted with p38α both endogenously and exogenously (**Supplementary Fig. 3d**). Deleting 153 residues from the N terminus (Nur77ΔN153) completely abolished p38α phosphorylation of Nur77 (**Supplementary Fig. 3e**), suggesting that the phosphorylated residues are in the TAD. The p38 phosphorylation motif, PXS/TP, was associated with residues Thr27 and Thr143 in the TAD. Two single point mutants (T27A and T143A) and a double point mutant (T27A T143A, referred to as the 2A mutant) were generated (**Supplementary Table 2**). p38α phosphorylation could still be detected in either the T27A or T143A mutants but not in the 2A mutant (**Fig. 3e** and **Supplementary Fig. 3f**), suggesting that both Thr27 and Thr143 are substrate sites for p38α.

Unexpectedly, 2A better inhibited NF-κB activity than either Nur77 (**Fig. 3f**) or a mutant that mimicked the phosphorylated Nur77 with both Thr27 and Thr143 mutated to glutamic acid (referred to as 2E). Transfection of 2A upon LPS stimulation in RAW264.7 cells resulted in lower TNF-α mRNA levels compared to that resulting from transfection of either Nur77 or 2E (**Supplementary Fig. 3g**). Taken together, it is a new phenomenon that p38α phosphorylation attenuates Nur77 inhibition of NF-κB activity, leading to a failure in the regulation of genes downstream of NF-κB.

PDNPA impedes the interaction between Nur77 and p38α

The above data indicate that p38α interacts with and subsequently phosphorylates Nur77. The LBD was shown to be the domain responsible for the direct interaction with p38α (**Supplementary Fig. 4a**). Disrupting this interaction may result in hypophosphorylation of Nur77 to suppress the LPS-induced inflammatory response. To this end, an in-house chemical library biased to the LBD was screened on the basis of NF-κB reporter activity in RAW264.7 cells. A compound, PDNPA (**Fig. 4a**), which has a high affinity to the LBD but not to p38α (**Supplementary Fig. 4b**), was identified as an inhibitor to LPS-stimulated NF-κB activity (**Fig. 4b**). The half-maximum inhibitory concentration (IC_{50}) of PDNPA on NF-κB activity is about 1.6 μM (**Supplementary Fig. 4c**). This value may not be consistent with its K_d value for Nur77, which might be due to the fact that PDNPA does not directly inhibit NF-κB activity. Instead, it interferes with the interaction between Nur77 and p38 to indirectly inhibit NF-κB activity. In addition, the half-maximal concentration of PDNPA inhibition on cell viability is 31.5 μM (**Supplementary Fig. 4d**), which indicates that PDNPA's anti-inflammatory role is independent of the induction of cell death. This PDNPA-associated suppression of NF-κB activity was Nur77 dependent. Once endogenous Nur77 was knocked down in RAW264.7 cells, PDNPA lost its capacity to suppress LPS-induced NF-κB reporter activity (**Fig. 4b**). However, PDNPA did not show any influence on Nur77 expression (**Supplementary Fig. 4e**) and stability (**Supplementary Fig. 4f**). PDNPA suppressed p65 binding to DNA in *Nur77*$^{+/+}$ but not *Nur77*$^{-/-}$ macrophages (**Fig. 4c**). Moreover, PDNPA evidently suppressed the expression of cytokines downstream of NF-κB, including TNF-α, IL-1β and IL-6, in *Nur77*$^{+/+}$ macrophages after LPS treatment but in neither LPS-stimulated *Nur77*$^{-/-}$ macrophages nor RAW264.7 cells with Nur77 knocked down (**Fig. 4d** and **Supplementary Fig. 4g**). Therefore, PDNPA inhibits p65 binding to DNA and NF-κB activation, probably by interfering with the cross-talk between Nur77 and p38α.

We excluded direct PDNPA attenuation of p38α kinase activity as the compound did not influence the elevation of p38α phosphorylation at Thr180 and Tyr182, an indicator for p38 activity, upon LPS stimulation (**Supplementary Fig. 4h**). Moreover, MK2, a substrate of p38α, was phosphorylated to a similar level before and after PDNPA treatment (**Supplementary Fig. 4i**). These

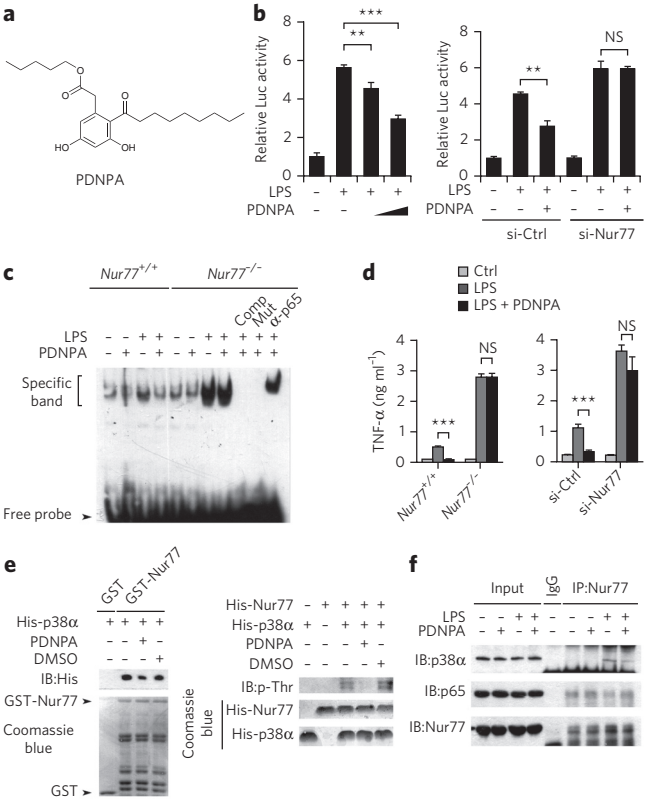

Figure 4 | PDNPA suppresses NF-κB activation by disrupting the interaction between p38α and Nur77. (**a**) The structure of PDNPA. (**b**) PDNPA inhibits LPS-induced NF-κB activity. Left, RAW264.7 cells were treated with LPS (100 ng ml^{-1}) and PDNPA (1 μM and 10 μM) for 9 h. Right, RAW264.7 cells were transfected with siRNA to Nur77 followed by LPS with or without PDNPA treatment (10 μM, 9 h). Luciferase assays were performed. Ctrl, control; NS, no significance. (**c**) PDNPA suppresses LPS-induced p65 binding to DNA. Peritoneal macrophages from WT or Nur77 KO mice were treated with LPS and PDNPA (1 h). Nuclear extracts were prepared for EMSA. Comp, competitor; Mut, mutant probe. (**d**) PDNPA suppresses the production of LPS-induced proinflammatory cytokine TNF-α. Peritoneal macrophages (left) or RAW264.7 cells transfected with siRNA (right) were treated with LPS and PDNPA (4 h). The culture medium was collected for analysis. (**e**) PDNPA blocks Nur77-p38α interaction and Nur77 phosphorylation. Recombinant Nur77 was incubated with His-p38α and either PDNPA (1 μM) or DMSO. GST pulldown (left) or the *in vitro* kinase assay (right) was carried out. IB, immunoblot. (**f**) PDNPA attenuates Nur77-p38α interaction in RAW264.7 cells. RAW264.7 cells were treated with LPS and PDNPA. Cell lysates were immunoprecipitated (IP) with anti-Nur77 antibody and analyzed by western blotting. Images of full blots are shown in **Supplementary Figure 8**. Representatives of three independent experiments with similar results are shown. Results are presented as the mean ± s.e.m. $^{**}P < 0.01$, $^{***}P < 0.001$. NS, no significance.

results indicate that PDNPA does not modulate p38α kinase activity. Nevertheless, PDNPA did influence the stability of the p38α–Nur77 complex. Preincubation of PDNPA reduced the association between Nur77 and p38α with an accompanying decrease in Nur77 phosphorylation (**Fig. 4e**). In contrast, PDNPA did not perturb the Nur77-p65 interaction (**Supplementary Fig. 4j**). PDNPA also disrupted the endogenous interaction between Nur77 and p38α, but not that between Nur77 and p65, under LPS stimulation in RAW264.7 cells (**Fig. 4f**). As a consequence, the LPS-induced phosphorylation of threonine in Nur77 was evidently suppressed by the addition of PDNPA (**Supplementary Fig. 4k**). All of these

data support the notion that PDNPA impedes the interaction between Nur77 and p38α but not between Nur77 and p65 to maintain the hypophosphorylation of Nur77. In conjunction with interfering with the interaction between Nur77 and p38α, PDNPA suppressed the LPS-induced production of proinflammatory cytokines in macrophages from $p38\alpha^{fl/fl}$ mice but not $LtrLys^{Cre}$-$p38\alpha^{\Delta/\Delta}$ mice (**Supplementary Fig. 4l**).

To analyze the selectivity of PDNPA, we separately knocked down expression of all three NR4A family members, Nur77 (NR4A1), Nurr1 (NR4A2) and NOR-1 (NR4A3), with siRNA. Only Nur77 knockdown effectively abolished PDNPA inhibition of NF-κB activity (**Supplementary Fig. 4m**) and p65 binding to DNA (**Supplementary Fig. 4n**). Although PDNPA still bound the LBDs of Nurr1 and NOR-1 (**Supplementary Fig. 4o**), no interaction between p38α and either Nurr1 or NOR-1 could be detected (**Supplementary Fig. 4p**). That PDNPA only binds nuclear receptors in the NR4A family, but not other nuclear receptors such as AR, ERα and RXRα (**Supplementary Fig. 4q**), is an indication that PDNPA selectively induces the anti-inflammatory functionality of Nur77 by interfering with the interaction between Nur77 and p38α.

PDNPA competes with p38α for LBD binding

The complex between LBD and PDNPA was made by soaking the crystalline protein with the compound. There are two unique LBD molecules (molecule I and molecule II) in the complex structure, each with a distinct conformation[25]. PDNPA binds molecule I with a more open conformation compared to its binding to molecule II (**Fig. 5a** and **Supplementary Fig. 5a**). No electron density was associated with PDNPA at the same location in molecule II, which is too narrow to accommodate the compound (**Supplementary Fig. 5b**). The binding site for PDNPA locates among helices H4, H5, H11 and H12 (**Fig. 5b**), which is distinct from the canonical ligand-binding site for the classical nuclear receptors.

Different mutations were made to perturb the PDNPA-LBD interaction. The single mutations L437W, S441W or D594E partially impaired PDNPA binding, whereas triple mutation of all three residues (referred to as LSD mut; **Supplementary Table 2**) completely abolished the interaction (**Supplementary Fig. 5c**). The crystal structures of the S441W and L437W D594E mutants showed that the introduction of bulkier residues excludes PDNPA binding (**Fig. 5c**). In contrast, additional single mutations at either H516W or P597W showed little interference in PDNPA binding to LBD (**Supplementary Fig. 5d**). Docking experiments suggest that the N terminus of p38α and PDNPA could bind at the same location in the LBD (**Fig. 5c,d**). Although the triple mutation perturbed the interaction with the compound, it did not interfere with the interaction between p38α and LBD (**Fig. 5d**). However, either H516W or P597W impaired the LBD interaction with p38α (**Fig. 5d**). GST pulldown assays further verified that mutation of either His516 or Pro597 impeded the p38α-LBD interaction, and LSD mutation did hamper, albeit not completely, this interaction (**Fig. 5e** and **Supplementary Fig. 5e**). It was also evident that PDNPA effectively obstructed the p38α association with LBD (**Fig. 5f**). Together, these data suggest that PDNPA competes with p38α binding to LBD to prevent the p38α phosphorylation of Nur77.

The crevice where PDNPA binds is also the binding site for a previously reported antidiabetic compound, ethyl 2-[2,3,4 trimethoxy-6(1-octanoyl)phenyl]acetate (TMPA)[25]. Although TMPA has a completely distinct function from PDNPA, in which it antagonizes Nur77's interaction with LKB1, there is only a subtle difference in binding modes between the two compounds (**Supplementary Fig. 5f**). This raises the question of whether there is cross-activity between TMPA and PDNPA. A series of

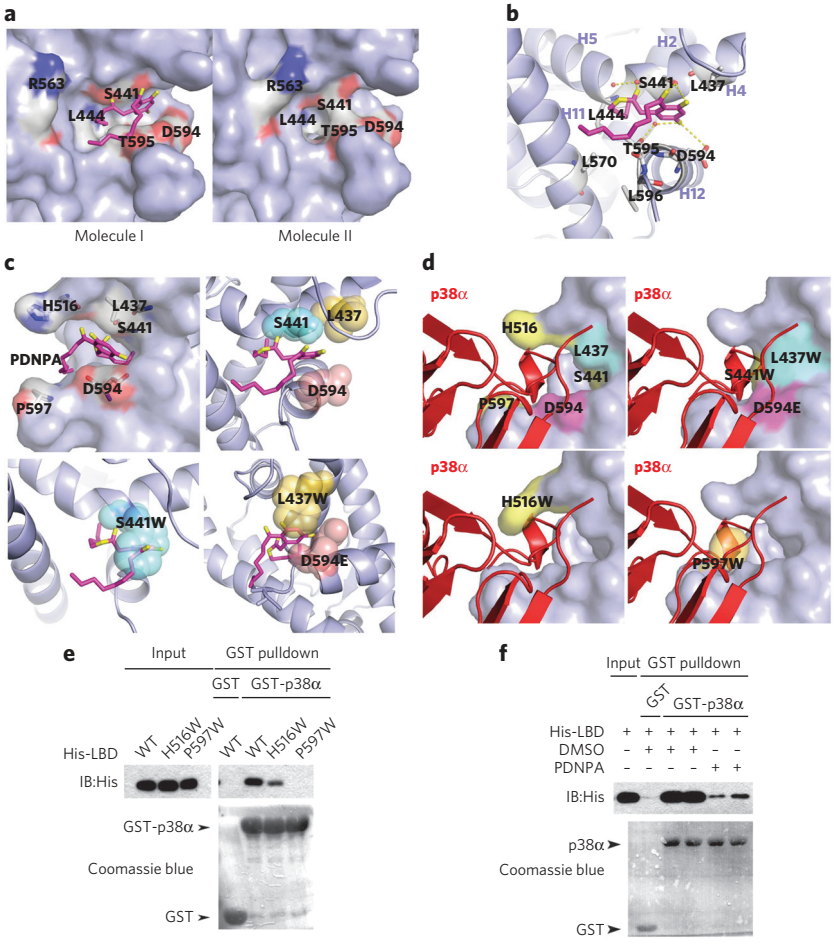

Figure 5 | Critical residues for PDNPA binding and p38α interaction. (**a**) PDNPA (purple) can be modeled only in molecule I but not the same location in molecule II, which has a different conformation. (**b**) PDNPA bound among H4, H5, H11 and H12 and interacted with residues L437, S441 and D594. Residues L444, L570 and L596 also provided the more hydrophobic environment for the ester alkyl chain and the acyl group in the compound. (**c**) Residues L437, S441 and D594 are at the bottom of PDNPA binding site. Mutation of S441 (bottom left) or double mutation of L437 and D594 prevents PDNPA from binding owing to space constraints (bottom right). (**d**,**e**) Critical residues in LBD for p38α binding. (**d**) Molecular docking shows the preferential p38α interaction with LBD at the same site with PDNPA binding (top left). Mutation of three residues (S441W, L437W and D594E) did not impair p38α binding (top right), whereas H516W and P597W did (bottom). IB, immunoblot. (**e**) A GST pulldown assay shows that P597 and H516 in the Nur77 LBD is important for p38 interaction. His-LBD and its different mutants were incubated with GST-p38α or GST *in vitro* and analyzed by western blotting. (**f**) PDNPA impairs the Nur77 LBD-p38α association. His-LBD was incubated with GST-p38α in the presence of either DMSO or PDNPA (1 μM) and analyzed by western blotting. Images of full blots are shown in **Supplementary Figure 8**. Representatives of three independent experiments with similar results are shown.

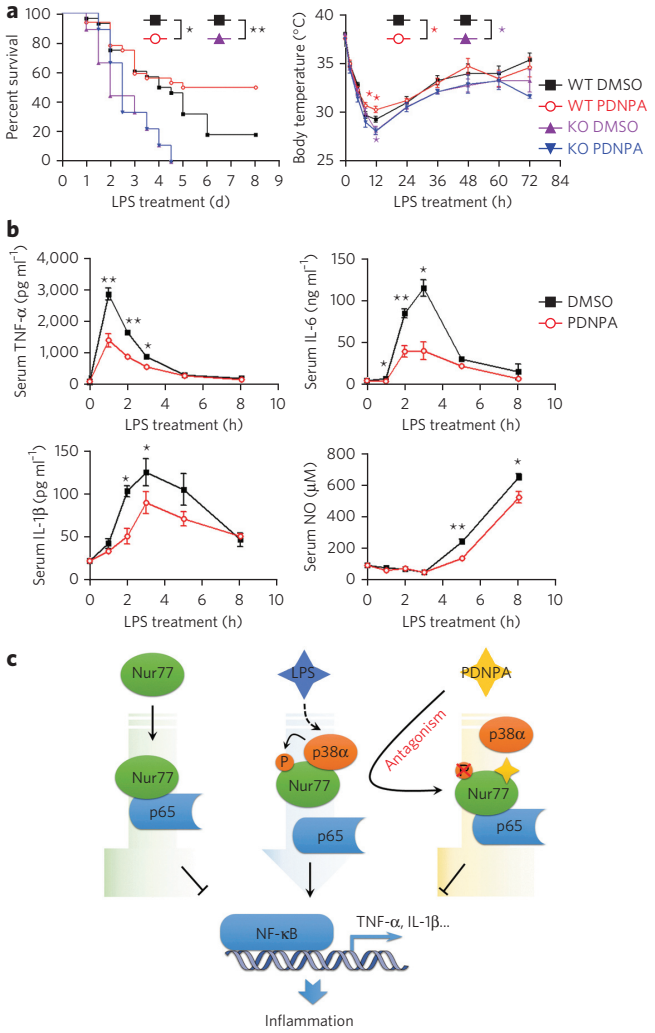

Figure 6 | PDNPA treatment for LPS- and CLP- induced sepsis. (**a**) PDNPA improved the survival rate of mice in LPS-induced sepsis. WT and KO mice were administered with PDNPA (50 mg per kg body weight, intravenous injection) for 2 h, followed by LPS (10 mg per kg body weight, intraperitoneal injection; $n = 15$). Survival rates (left) and body temperatures (right) were recorded at the times indicated. (**b**) PDNPA blocks the release of inflammatory mediators in the sera of WT mice. Mice were administrated with LPS and PDNPA as described above ($n = 6$). Sera were collected for the analysis of TNF-α, IL-6, IL-1β and NO. (**c**) An illustration on the regulatory role of Nur77 in NF-κB activity, p38α phosphorylation of Nur77 and PDNPA disruption of Nur77-p38α interaction in the LPS-induced inflammatory response. Kaplan-Meier plots were constructed, and statistical significance was analyzed by a log-rank test. Results are presented as the mean ± s.e.m. Representatives of two or three independent experiments with similar results are shown. $^*P < 0.05$, $^{**}P < 0.01$.

experiments was carried out to address this issue. First, although the mutation of either His516 or Pro597 impaired p38α binding (**Fig. 5d**), these mutations did not prevent LKB1 binding (**Supplementary Fig. 5g**). Structural hindrance from three bulky mutations in Ser441, Leu437 and Asp594 blocked PDNPA but not TMPA binding (**Supplementary Fig. 5f**). As expected, the T595E mutation, which affected LKB1 binding[25], did not interfere with p38α binding (**Supplementary Fig. 5g**). Second, TMPA increased the phosphorylation of AMPK in hepatic L02 cells, whereas PDNPA did not. Conversely, PDNPA suppressed LPS-induced TNF-α expression in macrophages, but TMPA did not (**Supplementary Fig. 5h**). Third, PDNPA weakened the interaction between p38α and LBD. In comparison, TMPA dampened the interaction between LKB1 and LBD, whereas PDNPA failed to do so (**Supplementary Fig. 5i**). Fourth, LBD mutations C566R and T595E impaired both TMPA and LKB1 binding[25] but neither p38α nor PDNPA binding (**Supplementary Fig. 5j**). In contrast, mutation of either H516W or P597W suppressed the p38α-LBD association but not the LKB1-LBD interaction. Furthermore, the triple mutant (LSD mut) lost the ability to bind PDNPA but not TMPA (**Supplementary Fig. 5k**). Finally, TMPA could not rescue mice from the lethal LPS challenge as PDNPA did, yet PDNPA was not capable of lowering the blood glucose in diabetic mice like TMPA (**Supplementary Fig. 5l**). It can be concluded that although both TMPA and PDNPA bind at the same location, the subtle difference in their binding is sufficient to induce completely different biological outcomes.

PDNPA effectively alleviates two models of sepsis

The physiological potential of PDNPA for treating sepsis was investigated by using mouse models mimicking the aforementioned two separate phases of sepsis. PDNPA treatment was sufficient to cause a decrease in the IL-6 concentration (**Supplementary Fig. 6a**) and significantly prolonged the lifespan of WT mice under LPS stimulation (**Fig. 6a**). WT mice with PDNPA treatment also had a higher body temperature within 12 h (**Fig. 6a**). However, neither survival rate nor body temperature in KO mice was affected by PDNPA, which corroborated the notion that Nur77 is required for PDNPA's attenuation of sepsis.

TNF-α and IL-6 in the sera of PDNPA-treated WT mice were significantly lower than those from the DMSO-treated controls in the first ~3–5 h after LPS injection. Concentrations of serum IL-1β and NO in PDNPA-treated mice arose more slowly and reached a lower peak compared to those of controls (**Fig. 6b**). This indicates that PDNPA administration suppresses the release of cytokines to attenuate LPS-induced endotoxic shock. Thus, PDNPA enhances mouse resistance to lethal sensitization from the LPS challenge.

PDNPA administration in CLP-induced sepsis increased the survival rate of WT mice but not KO mice (**Supplementary Fig. 6b**). As expected, PDNPA-treated WT mice, but not KO mice, had reduced bacteria levels and cytokine production (**Supplementary Fig. 6c,d**). Furthermore, LtrLys^{Cre}-p38α$^{Δ/Δ}$ mice were more resistant than p38α$^{fl/fl}$ mice to the lethality of LPS-induced sepsis[26], and PDNPA could rescue mice from lethality with the p38α$^{fl/fl}$ but not the LtrLys^{Cre}-p38α$^{Δ/Δ}$ genotype (**Supplementary Fig. 6e**). These results are consistent with the notion that LtrLys^{Cre}-p38α$^{Δ/Δ}$ mice had attenuated cytokine production compared to p38α$^{fl/fl}$ mice, and PDNPA reduced cytokine production in p38α$^{fl/fl}$ mice but not in LtrLys^{Cre}-p38α$^{Δ/Δ}$ mice (**Supplementary Fig. 6f**). Clearly, PDNPA attenuates both LPS- and CLP-induced sepsis via Nur77-p38α cross-talk.

DISCUSSION

The inflammatory response is a double-edged sword. An appropriate inflammatory response helps to remove pathogens, whereas an aggressive one leads to multiorgan dysfunction or even death. Therefore, understanding the precise regulatory mechanism in inflammatory response is critical to solve many inflammation-related diseases. In this study, Nur77 is shown to be a vital brake in the NF-κB–mediated inflammatory response. Knockout of Nur77 greatly sensitizes mice to LPS- and CLP-induced lethality. Nur77 could suppress NF-κB activity by blocking p65 binding to its κB element to attenuate the production of proinflammatory cytokines. This Nur77 function, however, is abolished by p38α phosphorylation upon LPS stimulation. PDNPA, a compound that binds the LBD, was identified to impede p38α phosphorylation of Nur77 by disrupting the Nur77-p38α interaction. This revealed that Nur77 carries out its anti-inflammatory role by regulating the p38α–NF-κB

pathway and identified an efficient compound to attenuate the inflammatory response (**Fig. 6c**).

As a check in the NF-κB pathway, Nur77 functions comparably or even complementarily in many aspects to IκB. IκB masks p65 in the cytosol to prevent NF-κB–associated transcription in the nucleus[27]. Nur77 locates in the nucleus of macrophages but also directly binds p65 to prevent its association with the κB element for transcription. IκB is ubiquitinated for degradation upon phosphorylation by IKKs, which activates NF-κB. p38α phosphorylation dampens the Nur77 interaction with p65 to relieve the suppression of NF-κB activity. Both IκB and Nur77 are involved in the autoregulation of NF-κB. IκBα entry to the nucleus leads to the inactivation of DNA-bound NF-κB for export to the cytoplasm[28,29]. Elevated expression of Nur77 results in the suppression of NF-κB activity. Moreover, Nur77 was reported to increase IκBα expression in vascular endothelial cells (human umbilical vein endothelial cells)[15], which, however, seems to be cell line and stimuli dependent.

p38α phosphorylates many transcription factors that control the expression of proinflammatory cytokines[30,31]. This study demonstrates a new p38α regulatory mechanism, in which phosphorylation of Nur77 modulates the NF-κB activity and the production of proinflammatory cytokines. We demonstrated that phosphorylation is an important regulatory mechanism for Nur77 functions[32,33]. In macrophages, p38α phosphorylates Nur77 at residues Thr27 and Thr143 upon LPS stimulation to diminish Nur77 suppression of NF-κB activity, and these are the same residues that are also phosphorylated by GSK3β in intestinal tumorigenesis for attenuating Nur77's inhibition on Wnt activity[34]. Thus, the phosphorylation of Nur77 at the same site by different kinases upon different types of stimulation can result in different biological outcomes.

There is no physiological ligand for Nur77 identified to date. Regulatory compounds targeting Nur77, however, do exist. We demonstrated that Csn-B agonized the transactivation activity of Nur77 by binding the LBD[35]. A Csn-B derivative, 1-(3,4,5-trihydroxyphenyl) nonan-1-one (THPN), interacted with the LBD to provide a suitable surface for Nur77's interaction with Nix, leading to Nur77 translocation to the mitochondria to induce autophagic cell death in melanoma[36]. Another Csn-B derivative, TMPA, also binds the LBD to block the interaction between Nur77 and LKB1, facilitating LKB1 shuttling to the cytoplasm to activate AMPK activity and decrease the glucose level in diabetic mice[25]. In the current study, neither TMPA nor THPN influences the NF-κB transcription activity in RAW264.7 cells or mouse survival in the sepsis models. Csn-B slightly inhibits the NF-κB transcription activity in RAW264.7 cells but showed no obvious effect on LPS-induced mouse sepsis (**Supplementary Fig. 7**). Conversely, PDNPA is an effective anti-inflammatory compound that disrupted the interaction between Nur77 and p38 to block the p38-activated NF-κB signaling pathway. These Nur77-targeting compounds directly influence the interactions between Nur77 and its interacting partners in a new paradigm that is distinct from physiological ligand binding at the canonical ligand-binding pocket in traditional nuclear receptors. Though these compounds share similarities in chemical structure, they have diverse yet specific and nonoverlapping functions. Their discovery paves the way for designing new therapeutics to treat various diseases.

PDNPA is a competitive inhibitor to the Nur77-p38 interaction rather than an antagonist in the traditional sense as it does not bind the canonical pocket. PDNPA is not Nur77 specific as it also binds both Nurr1 and NOR-1. However, PDNPA's functional readout on the p38 pathway is Nur77 specific, as only the knockdown of Nur77 abolished the activity of PDNPA. The binding of PDNPA to either Nurr1 or NOR-1 has no phenotypic consequence as neither of them interact with p38. In light of the fact that PDNPA does not bind other nuclear receptors such as AR, ERα or RXRα, PDNPA is highly specific for Nur77-associated regulation of the p38α–NF-κB pathway.

Steroidal compounds (such as glucocorticoids) and nonsteroidal compounds (such as coxibs) are widely used to treat inflammation. However, their safety issues concerning gastrointestinal or cardiovascular applications cannot be ignored[37,38]. Developing more effective and less toxic agents to treat acute and chronic inflammatory diseases is still a challenge[39]. As it has a critical role in regulating the production of proinflammatory cytokines, p38 is a highly valued therapeutic target for treating inflammatory diseases. The general approach is to develop inhibitors targeting its ATPase activity; by 2007, about 20 of these had progressed to clinical trials. To date, however, only SCIO469 and VX702 remain in phase II trials[40–42] owing to unacceptable safety profiles[43–45]. Impeding the specific interaction between p38 and its substrates is an alternative approach to reduce the clinical attrition of p38 inhibitors. For example, the aniline analog CMPD1 was identified to bind p38α and selectively inhibit p38α activity toward the substrate MK2 (ref. 46). Nur77 is a new substrate for p38α, and PDNPA is a potential anti-inflammatory compound, competing with p38α for Nur77 binding. This specific PDNPA property thus provides a unique framework for developing anti-inflammatory drugs with few side effects.

Received 14 November 2014; accepted 2 March 2015; published online 30 March 2015

METHODS

Methods and any associated references are available in the online version of the paper.

Accession codes. Protein Data Bank (PDB): The coordinates and the structure factors were deposited under accession codes 4RZG for PDNPA-bound NUR77 LBD at 2.7-Å resolution, 4RZE for NUR77 LBD$^{L437W\ D594E}$ at 2.49-Å resolution and 4RZF for NUR77 LBD^{S441W} at 1.99-Å resolution.

References

1. Lever, A. & Mackenzie, I. Sepsis: definition, epidemiology, and diagnosis. *Br. Med. J.* **335**, 879–883 (2007).
2. Hartman, M.E., Linde-Zwirble, W.T., Angus, D.C. & Watson, R.S. Trends in the epidemiology of pediatric severe sepsis. *Pediatr. Crit. Care Med.* **14**, 686–693 (2013).
3. Ulloa, L. & Tracey, K.J. The "cytokine profile": a code for sepsis. *Trends Mol. Med.* **11**, 56–63 (2005).
4. Beutler, B. & Rietschel, E.T. Innate immune sensing and its roots: the story of endotoxin. *Nat. Rev. Immunol.* **3**, 169–176 (2003).
5. Akira, S. & Takeda, K. Toll-like receptor signalling. *Nat. Rev. Immunol.* **4**, 499–511 (2004).
6. Han, J. & Ulevitch, R.J. Limiting inflammatory responses during activation of innate immunity. *Nat. Immunol.* **6**, 1198–1205 (2005).
7. Hayden, M.S. & Ghosh, S. Signaling to NF-κB. *Genes Dev.* **18**, 2195–2224 (2004).
8. Beyaert, R. *et al.* The p38/RK mitogen-activated protein kinase pathway regulates interleukin-6 synthesis response to tumor necrosis factor. *EMBO J.* **15**, 1914–1923 (1996).
9. Vanden Berghe, W. *et al.* p38 and extracellular signal-regulated kinase mitogen-activated protein kinase pathways are required for nuclear factor-κB p65 transactivation mediated by tumor necrosis factor. *J. Biol. Chem.* **273**, 3285–3290 (1998).
10. Ono, K. & Han, J. The p38 signal transduction pathway: activation and function. *Cell. Signal.* **12**, 1–13 (2000).
11. Saha, R.N., Jana, M. & Pahan, K. MAPK p38 regulates transcriptional activity of NF-κB in primary human astrocytes via acetylation of p65. *J. Immunol.* **179**, 7101–7109 (2007).
12. Hazel, T.G., Nathans, D. & Lau, L.F. A gene inducible by serum growth factors encodes a member of the steroid and thyroid hormone receptor superfamily. *Proc. Natl. Acad. Sci. USA* **85**, 8444–8448 (1988).
13. Pei, L., Castrillo, A., Chen, M., Hoffmann, A. & Tontonoz, P. Induction of NR4A orphan nuclear receptor expression in macrophages in response to inflammatory stimuli. *J. Biol. Chem.* **280**, 29256–29262 (2005).
14. Bonta, P.I. *et al.* Nuclear receptors Nur77, Nurr1, and NOR-1 expressed in atherosclerotic lesion macrophages reduce lipid loading and inflammatory responses. *Arterioscler. Thromb. Vasc. Biol.* **26**, 2288–2294 (2006).

15. You, B., Jiang, Y.Y., Chen, S., Yan, G. & Sun, J. The orphan nuclear receptor Nur77 suppresses endothelial cell activation through induction of IκBα expression. *Circ. Res.* **104**, 742–749 (2009).
16. Hamers, A.A. *et al.* Bone marrow–specific deficiency of nuclear receptor Nur77 enhances atherosclerosis. *Circ. Res.* **110**, 428–438 (2012); erratum **110**, e46 (2012).
17. Hanna, R.N. *et al.* NR4A1 (Nur77) deletion polarizes macrophages toward an inflammatory phenotype and increases atherosclerosis. *Circ. Res.* **110**, 416–427 (2012).
18. Doi, K., Leelahavanichkul, A., Yuen, P.S. & Star, R.A. Animal models of sepsis and sepsis-induced kidney injury. *J. Clin. Invest.* **119**, 2868–2878 (2009).
19. Litvak, V. *et al.* Function of C/EBPΔ in a regulatory circuit that discriminates between transient and persistent TLR4-induced signals. *Nat. Immunol.* **10**, 437–443 (2009).
20. Tian, B., Nowak, D.E., Jamaluddin, M., Wang, S. & Brasier, A.R. Identification of direct genomic targets downstream of the nuclear factor-κB transcription factor mediating tumor necrosis factor signaling. *J. Biol. Chem.* **280**, 17435–17448 (2005).
21. Németh, Z.H. *et al.* cDNA microarray analysis reveals a nuclear factor-κB–independent regulation of macrophage function by adenosine. *J. Pharmacol. Exp. Ther.* **306**, 1042–1049 (2003).
22. Wang, H. *et al.* NF-κB regulation of YY1 inhibits skeletal myogenesis through transcriptional silencing of myofibrillar genes. *Mol. Cell. Biol.* **27**, 4374–4387 (2007).
23. Alkalay, I. *et al.* Stimulation-dependent IκBα phosphorylation marks the NF-κB inhibitor for degradation via the ubiquitin-proteasome pathway. *Proc. Natl. Acad. Sci. USA* **92**, 10599–10603 (1995).
24. Hong, C.Y. *et al.* Molecular mechanism of suppression of testicular steroidogenesis by proinflammatory cytokine tumor necrosis factor α. *Mol. Cell. Biol.* **24**, 2593–2604 (2004).
25. Zhan, Y.Y. *et al.* The orphan nuclear receptor Nur77 regulates LKB1 localization and activates AMPK. *Nat. Chem. Biol.* **8**, 897–904 (2012).
26. Kang, Y.J. *et al.* Macrophage deletion of p38α partially impairs lipopolysaccharide-induced cellular activation. *J. Immunol.* **180**, 5075–5082 (2008).
27. Malek, S., Huxford, T. & Ghosh, G. IκBα functions through direct contacts with the nuclear localization signals and the DNA binding sequences of NF-κB. *J. Biol. Chem.* **273**, 25427–25435 (1998).
28. Sun, S.C., Ganchi, P.A., Ballard, D.W. & Greene, W.C. NF-κB controls expression of inhibitor IκBα: evidence for an inducible autoregulatory pathway. *Science* **259**, 1912–1915 (1993).
29. Arenzana-Seisdedos, F. *et al.* Nuclear localization of IκBα promotes active transport of NF-κB from the nucleus to the cytoplasm. *J. Cell Sci.* **110**, 369–378 (1997).
30. Han, J., Lee, J.D., Bibbs, L. & Ulevitch, R.J.A. MAP kinase targeted by endotoxin and hyperosmolarity in mammalian cells. *Science* **265**, 808–811 (1994).
31. Trempolec, N., Dave-Coll, N. & Nebreda, A.R. SnapShot: p38 MAPK substrates. *Cell* **152**, 924–924 e1 (2013).
32. Liu, B. *et al.* Regulation of the orphan receptor TR3 nuclear functions by c-Jun N terminal kinase phosphorylation. *Endocrinology* **148**, 34–44 (2007).
33. Wang, A., Rud, J., Olson, C.M. Jr., Anguita, J. & Osborne, B.A. Phosphorylation of Nur77 by the MEK-ERK-RSK cascade induces mitochondrial translocation and apoptosis in T cells. *J. Immunol.* **183**, 3268–3277 (2009).
34. Chen, H.Z. *et al.* The orphan receptor TR3 suppresses intestinal tumorigenesis in mice by downregulating Wnt signalling. *Gut* **61**, 714–724 (2012).
35. Liu, J.J. *et al.* A unique pharmacophore for activation of the nuclear orphan receptor Nur77 *in vivo* and *in vitro*. *Cancer Res.* **70**, 3628–3637 (2010).
36. Wang, W.J. *et al.* Orphan nuclear receptor TR3 acts in autophagic cell death via mitochondrial signaling pathway. *Nat. Chem. Biol.* **10**, 133–140 (2014).
37. Dogné, J.M., Supuran, C.T. & Pratico, D. Adverse cardiovascular effects of the coxibs. *J. Med. Chem.* **48**, 2251–2257 (2005).
38. Mukherjee, D., Nissen, S.E. & Topol, E.J. Risk of cardiovascular events associated with selective COX-2 inhibitors. *J. Am. Med. Assoc.* **286**, 954–959 (2001).
39. Dinarello, C.A. Anti-inflammatory agents: present and future. *Cell* **140**, 935–950 (2010).
40. Peifer, C., Wagner, G. & Laufer, S. New approaches to the treatment of inflammatory disorders small molecule inhibitors of p38 MAP kinase. *Curr. Top. Med. Chem.* **6**, 113–149 (2006).
41. Hynes, J. Jr. & Leftheri, K. Small molecule p38 inhibitors: novel structural features and advances from 2002–2005. *Curr. Top. Med. Chem.* **5**, 967–985 (2005).
42. Pettus, L.H. & Wurz, R.P. Small molecule p38 MAP kinase inhibitors for the treatment of inflammatory diseases: novel structures and developments during 2006–2008. *Curr. Top. Med. Chem.* **8**, 1452–1467 (2008).
43. Genovese, M.C. Inhibition of p38: has the fat lady sung? *Arthritis Rheum.* **60**, 317–320 (2009).
44. Zhang, J., Shen, B. & Lin, A. Novel strategies for inhibition of the p38 MAPK pathway. *Trends Pharmacol. Sci.* **28**, 286–295 (2007).
45. Goldstein, D.M. & Gabriel, T. Pathway to the clinic: inhibition of P38 MAP kinase. A review of ten chemotypes selected for development. *Curr. Top. Med. Chem.* **5**, 1017–1029 (2005).
46. Davidson, W. *et al.* Discovery and characterization of a substrate selective p38αinhibitor. *Biochemistry* **43**, 11658–11671 (2004).

Acknowledgments

This work was supported by grants from the National Natural Science Fund of China, the '973' Project of the Ministry of Science and Technology (91413113, 2014CB910602, 31370724, 31221065) and the Program of Introducing Talents of Discipline to Universities (B12001). The crystallographic data collection at Beamline BL17U1 at Shanghai Synchrotron Radiation Facility is gratefully acknowledged.

Author contributions

The Wu laboratory (L.L., Y.L., H.C., J. He, Y.X., Y.C. and W.W.) was responsible for the experiments on molecular cellular biology and detection in mice. The Lin laboratory (F.L., X.T., A.L., Q.Z.) was responsible for the structure determination and analysis. The Han laboratory (J.W.) provided $p38\alpha^{fl/fl}$ and $LtrLys^{Cre}$-$p38\alpha^{\Delta/\Delta}$ mice. The Huang laboratory (H.Z.) provided the compounds. J. Han was involved in the discussion of the manuscript. Q.W. and T.L. designed the experiments and wrote the manuscript.

Competing financial interests

The authors declare no competing financial interests.

Additional information

Supplementary information and chemical compound information is available in the online version of the paper. Reprints and permissions information is available online at http://www.nature.com/reprints/index.html. Correspondence and requests for materials should be addressed to T.L. or Q.W.

ONLINE METHODS

Cell culture, transfection and drugs. Human embryonic kidney (HEK293T) cells and mouse monocyte/macrophage RAW264.7 cells were purchased from the Institute of Cell Biology, China. Human liver cell line (L02) was purchased from Cell Bank in Chinese Academy of Sciences in Kunming. Cell lines were cultured in Dulbecco's Modified Eagle's Medium (for 293T and RAW 264.7 cell lines) or RPMI-1640 medium (for L02 cell line) supplemented with 10% FBS (FBS; Hyclone, Logan, UT), 100 U penicillin and 100 μg/ml streptomycin. Transfection was carried out by using FuGENE HD transfection reagent (Promega, Madison, WI) according to the manufacturer's instructions. Lipopolysaccharide (LPS, *E. coli* 0111:B4, Sigma) was dissolved in PBS.

PDNPA was dissolved in DMSO. Different doses of PDNPA were used to test NF-κB transcription activity, and 10 μM PDNPA was determined to be suitable for the study. The concentration of TMPA was determined as reported[25].

Plasmids construction. pGL6-NF-κB-Luc reporter with four NF-κB response elements (GGGAATTTCC) inserted into the pGL6-TA vector was purchased from the Beyotime Institute of Biotechnology (cat. no. D2207). Human p38α constructs with either a Flag or GST tag were generous gifts from J. Han at Xiamen University. Human p65, Nur77, Nurr1, NOR-1 and their deletions were constructed with either pCMV5-HA or pET-22b vectors.

Experimental animal models. Wild-type and Nur77-KO mice (C57BL/6J background) were purchased from the Jackson Laboratory. LtrLys^{Cre}-p38α$^{Δ/Δ}$ and p38α$^{fl/fl}$ mice were provided by J. Han (Xiamen University, China)[26]. Mice were maintained in 12-h light/12-h dark cycles with free access to food and water. PDNPA and TMPA were dissolved in DMSO to a final concentration of 1 M and diluted with 5.0% (v/v) Tween-80 and 0.9%(w/v) saline. DMSO in 5.0% (v/v) Tween-80 and 0.9% (w/v) saline was used as the vehicle control. All procedures were performed in compliance with the guidelines from the Institutional Animal Care and Use Committee at Experimental Animal Centre in Xiamen University (acceptance no. XMULAC20120030).

Mouse model for LPS-induced sepsis. Eight-week-old WT and KO mice were intraperitoneally injected with 10 mg per kg body weight LPS. After injection, body temperatures and survival rates were recorded. Serum and tissue samples were collected as required. To test efficacy, mice were intravenously injected with either PDNPA (50 mg per kg body weight) or TMPA (50 mg per kg body weight) 2 h before LPS injection (10 mg per kg body weight).

Mouse model for CLP-induced sepsis. Eight-week-old mice were weighed and anesthetized. Lower quadrants of the abdomen were shaved, and a skin midline incision was made. The cecum of each mouse was ligated in the middle and perforated by a single through-and-through puncture midway between the ligation and the tip of the cecum with a 21G needle. After removing the needle, the cecum was extruded with a small amount of feces and then relocated. The peritoneum of mice was then closed and resuscitated by injecting prewarmed saline (37 °C, 1 ml per mouse) subcutaneously. The mice were placed back in cages and monitored every 6 h after the operation. Sham mice underwent a similar procedure as CLP mice, including anesthetizing and abdominal midline incision, with the exception that the cecum in shams was not manipulated. For PDNPA administration, PDNPA (50 mg per kg body weight) was intravenously injected after the operation.

HFD/STZ-induced mice with type II diabetes. To induce diabetes, WT C57BL/6J mice (8-week-old) were fed a high-fat diet (HFD; Research Diets) containing 60% kcal from fat. After 4 weeks of dietary manipulation, mice were treated with a low dose of STZ (Sigma; 35 mg per kg body weight dissolved in 0.1 M sodium citrate buffer, pH 4.5) once daily for 7 d. To evaluate whether type II diabetes was established in the mice, blood glucose was monitored, and frank hyperglycemia was observed in HFD-induced mice but not in normal diet–fed mice after STZ treatment. The diabetic mice were treated with TMPA (50 mg per kg body weight) or PDNPA (50 mg per kg body weight) by intraperitoneal injection once daily for 19 days, and the blood glucose of the mice was analyzed at the times indicated in **Supplementary Figure 5l** after fasting for 12 h.

Isolation and culture of peritoneal macrophages. Three days before isolation, mice were intraperitoneally injected with 2 ml 4% thioglycollate medium (BD). Peritoneal macrophages were collected by peritoneal lavage with 10 ml cold PBS. Cells were incubated in DMEM supplemented with 10% FBS at 37 °C for 2 h and washed with PBS to eliminate nonadherent cells. The adherent cells were used as peritoneal macrophages.

Assay for inflammatory indicators and cytokines. Blood urea nitrogen (BUN) and nitric oxide (NO) levels were determined using commercially available kits (Nanjing Jiancheng Bioengineering Institute, Nanjing, China) according to the manufacturer's instructions. The concentrations of TNF-α, IL-6 and IL-1β were determined using ELISA kits (eBioscience, San Diego, CA) according to the manufacturer's instructions.

The kinase assay *in vitro*. Purified GST-Nur77 or its mutants were incubated with pure His-p38α in a 50-μl reaction mixture containing 25 mM Tris-HCl (pH 7.4), 10 mM magnesium chloride, 5 mM β-glycerol phosphate, 1 mM dithiothreitol (DTT), 0.1 mM sodium orthovanadate and 50 μM ATP. The mixture was incubated at 30 °C for 30 min. The reaction was terminated with the loading buffer for SDS-PAGE.

Nuclear extracts and EMSA. Cells were lysed in 100 μl Buffer A (10 mM HEPES, pH 7.9, 10 mM KCl, 0.1 mM EDTA, 0.1 mM EGTA, 0.15% NP-40) and 1% protease inhibitor for 15 min and centrifuged at 12,000*g* for 30 min at 4 °C. The pellet was washed three times with 1 ml Buffer A, resuspended in 150 μl Buffer B (20 mM HEPES, pH 7.9, 0.4 mM NaCl, 1 mM EDTA, 1 mM EGTA, 0.5% NP-40) containing 1% protease inhibitor and sonicated. The supernatant was used as the nuclear fraction.

To analyze the relationship between p38α phosphorylation of Nur77 and p65 binding of DNA, bacterially expressed Nur77 was phosphorylated by Ni-bound p38α as described in the kinase assay, with removal of p38α by precipitation. The supernatant was used as phosphorylated Nur77 in EMSA. Nur77 incubated with Ni-NTA beads was used as the control.

The κB element and its mutant were labeled with biotin at both ends, and EMSA was carried out according to the manufacturer's protocols (Pierce). The gel shift was detected by using a LightShift Chemiluminescent EMSA Kit (Thermo) according to the manufacturer's instructions.

The κB element without biotin labeling was used as the competitor (5′-3′):

κB element: AGTTGAGGGGACTTTCCCAGGC
κB mutant: AGTTGAGGCGACTTTCCCAGGC

Co-IP and western blotting analysis. Cells were lysed in modified ELB (150 mM NaCl, 100 mM NaF, 50 mM Tris-HCl, pH 7.6, 0.5% Nonidet P-40 (NP-40) and 1 mM PMSF) or lysis buffer (50 mM HEPES, pH 7.4,100 mM NaCl,10% glycerol,1% Triton X-100, 1.5 mM MgCl2, 25 mM NaF and 1 mM PMSF). Cell lysates were incubated with the appropriate antibody together with protein A–Sepharose beads for 3 h. The protein-antibody complexes on the beads were subjected to western blotting analysis. Mouse anti-HA (cat. no. H-9658, 1:5,000 for western blotting), anti-Flag (cat. no. F-1804, 1:5,000 for western blotting) and anti-β-tubulin (cat. no. T4026, 1:5,000 for western blotting) antibodies were purchased from Sigma. Rabbit anti-Myc (cat. no. SC-789, 1:1,000 for western blotting), mouse anti-GFP (cat. no. SC-9996, 1:1,000 for western blotting), rabbit anti-p65 (cat. no. SC-372, 1:1,000 for western blotting) and rabbit anti-IκBα (cat. no. SC-371, 1:1,000 for western blotting) antibodies were purchased from Santa Cruz Biotechnology. Rabbit anti-phosphothreonine (cat. no. 9381S, 1:1,000 for western blotting), anti-p38 (cat. no. 9212S, 1:1,000 for western blotting), anti-phospho-p38 T180/Y182 (cat. no. 4511S, 1:1,000 for western blotting), anti-Nur77 (cat. no. 3960S, 1:1,000 for western blotting), anti-phospho-JNK (cat. no. 9255S, 1:1,000 for western blotting) and anti-phospho-IKKα/β (cat. no. 2697P, 1:1,000 for western blotting) antibodies were purchased from Cell Signaling Technology. Rabbit anti-phosphoserine antibody (cat. no. 618100, 1:2,000 for western blotting) was purchased from Invitrogen.

Luciferase reporter assay. Cells were transfected with the pGL6-NFκB-Luc reporter constructs, β-galactosidase (β-gal) expression vectors and other relevant plasmids. Twenty-four hours after transfection, the luciferase activity was measured and normalized for transfection efficiency to internal β-gal activity.

The GST pulldown assay *in vitro*. GST or GST-fusion proteins were expressed in *E. coli* strain BL21 and purified using glutathione-Sepharose (Sigma). His-fusion proteins were expressed in *E. coli* strain BL21 and purified using Ni-NTA agarose (Qiagen). The bead-bound GST or GST-fusion proteins were incubated with 500 ng His-tagged protein in 400 μl modified ELB buffer (150 mM NaCl, 100 mM NaF, 50 mM Tris-HCl, pH 7.6, 0.5% Nonidet P-40 (NP-40) and 1 mM PMSF) at 4 °C for 1 h. Unbound proteins were removed by washing with

modified ELB buffer three times. The proteins were eluted by boiling in loading buffer for 10 min for SDS-PAGE.

Real-time PCR. Total RNA was extracted using the RNeasy kit (Qiagen) and reverse transcribed with M-MuLV reverse transcriptase (Fermentas). cDNA was amplified using primers specific for Tnf-α and Actin mRNA. Real-time PCR was performed using Sybr Green–based detection in the Rotor-Gene according to the manufacturer's instruction. Actin mRNA levels were used as the controls for normalization. The primers were as below (5′-3′):

Tnf-α: forward, AGCCCACGTCGTAGCAAACCA; reverse, CGGGGC AGCCTTGTCCCTTG

Actin: forward, CAGCCTTCCTTCCTGGGCATG; reverse, ATTGTG CTGGGTGCCAGGGCAG

16s rRNA; forward, GTGGTGCATGGTTGTCGTCA; reverse, ACGTCG TCCCCACCTTCCTC

Microarrays and GSEA. Peritoneal macrophages (*Nur77*$^{+/+}$ and *Nur77*$^{-/-}$) were isolated from WT and Nur77 KO mice, respectively ($n = 3$). After LPS treatment (100 ng/ml, 1 h), cells were harvested for RNA extraction using TRIzol reagent (Invitrogen). The microarrays were carried out by China National Engineering Center for Biochip at Shanghai. Heat maps were generated through the SBS Analysis System (http://sas.ebioservice.com/).

Gene expression data from *Nur77*$^{+/+}$ and *Nur77*$^{-/-}$ macrophages (three WT mice versus three KO mice) were used as inputs for the GSEA analysis. The GSEA software v2.0.14 (http://www.broadinstitute.org/gsea/)[47] was used for the GSEA analysis. Gene sets were either obtained from the MSigDB database v4.0 or from published gene signatures. Statistical significance was assessed by comparing the enrichment score to enrichment results generated from 1,000 random permutations of the gene set to obtain *P* values (nominal *P* value).

Crystallization, data collection and processing. Crystals of apo LBD of Nur77 and its mutants were obtained at 16 °C by hanging-drop vapor diffusion. The droplets consisted of a 1:1 (v/v) mixture of LBD at 6 mg/ml and the well solution of 100 mM sodium citrate, pH4.2, 20% glycerol and 7.5% PEG4000. Crystals appeared after 36–48 h and were ready for data collection in 14 d. For the formation of the complexes, crystals were soaked in a reservoir solution containing an additional 0.5 mM PDNPA before being transferred to a cryo-solution comprising the reservoir solution and 5% (v/v) glycerol, 1.5% (v/v) PEG4000 and 0.75 mM PDNPA and then were incubated for 3 h. The crystals were flash-cooled in liquid nitrogen to −170 °C. The diffraction data were collected at 100 K under the synchrotron radiation at beamline BL17U1 of the Shanghai Synchrotron Radiation Facility (SSRF). The data sets were integrated and scaled with the HKL2000 package.

The structures of LBD, its mutants and its complexes with PDNPA were determined by molecular replacement with the structure of LBD (PDB accession code 3V3E) as the initial search model with the program Phaser[48]. The programs Refmac5 and Coot9 (ref. 49) in the CCP4 suite[50–52] were used for the refinement and model building. Ramachandran plots were generated with Coot9. The statistics for data processing and structure refinement are shown in **Supplementary Table 2**.

Fluorescence quenching assay. Fluorescence spectra were obtained as previously described[25]. Briefly, His-fusion proteins were expressed in *E. coli* strain BL21, purified and dialyzed against PBS (pH 7.4). For analyzing the interactions between the protein and compounds, 5 μM proteins were incubated with various concentrations of compounds, and fluorescence quenching was monitored at 25 °C with a slit width of 5 nm for excitation and a slit width of 2.5 nm for emission. The excitation wavelength was 280 nm, and the emission spectra were recorded from 285 nm to 410 nm. To estimate the binding affinity, the fluorescence intensities at 334 nm with increasing concentrations of quencher were measured, and the values of K_d were calculated according to the law of mass action formula[53].

Modeling the interaction between Nur77 and p38α. Coordinates for the LBD (PDB code 3V3E) and p38α (PDB code 1M7Q) were obtained from the PDB for docking with the program ZDOCK[54] implemented in Discovery Studio 3.1 (Accelrys Software Inc., San Diego), which modeled and simulated the interactions between two molecules. LBD was the receptor, and p38α was the ligand. The docking poses were clustered on the basis of the all-atom r.m.s. deviation of any two ligands. Poses from each cluster with high ZDock Scores were selected and minimized by RDOCK[55] using the CHARMm force field[56]. One complex structure with p38α located in LBD of Nur77 was identified in the top ten binding poses ranked by E_RDock value. The complex was further optimized using molecular dynamics simulations by the Desmond program, version 3.1 (Schrödinger, New York) using the OPLS2005 force field[57,58], which performed high-speed molecular dynamics simulations of biological systems on conventional commodity clusters. The LBD and p38α complex were solvated in TIP3P water molecules using an orthorhombic box that can fit the molecule with a 12-Å buffer zone. The system was neutralized by the addition of Na^+ ions. The systems were relaxed before simulation by using the default Desmond protocol. A 2-ns simulation was carried out using the NPT ensemble with a target pressure of 1.0132 bar and a temperature of 300 K.

Statistical analysis. Survival curves were analyzed by Kaplan-Meier using a log-rank test. Data are expressed as mean ± s.e.m. The differences between two groups were assessed by a two-tailed unpaired Student's *t*-test or by one-way or two-way ANOVA with SPSS software (version 13; SPSS Inc., Chicago, IL).

Synthesis of PDNPA. Synthetic PDNPA was fully characterized by ^{1}H NMR, ^{13}C NMR, MS and elemental analysis. A summary of the synthetic procedure of PDNPA is as follows[35]:

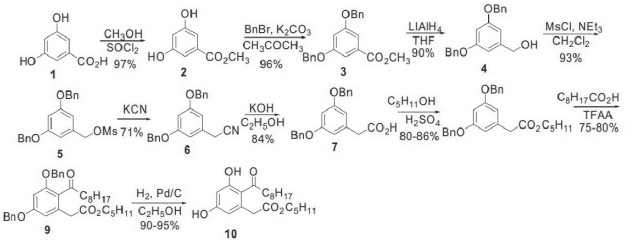

PDNPA is a white solid with melting point 97–98 °C; IR (film): 3,334 cm^{-1}, 2,956 cm^{-1}, 2,927 cm^{-1}, 2,856 cm^{-1}, 1,708 cm^{-1}, 1,614 cm^{-1}, 1,591 cm^{-1}, 1,466 cm^{-1}, 1,416 cm^{-1}, 1,377 cm^{-1}, 1,329 cm^{-1}, 1,260 cm^{-1}, 1,162 cm^{-1}, 1,112 cm^{-1}, 1,046 cm^{-1}, 1,017 cm^{-1}; ^{1}H NMR (400 MHz, $CDCl_3$) δ 0.88 (t, J = 6.9 Hz, 3H, -CH_3), 0.90 (t, J = 7.0 Hz, 3H, -CH_3), 1.18–1.37 (m, 14H, 7 × CH_2), 1.59–1.74 (m, 4H, 2 × CH_2), 2.83 (t, J = 7.4 Hz,2H,-CH_2CO), 3.83 (s, 2H, -CH_2CO), 4.13 (t, J = 6.8 Hz, 2H, -CH_2-), 6.26 (d, J = 2.4 Hz, 1H, ArH), 6.27 (d, J = 2.4 Hz, 1H, ArH), 6.46 (brs, 1H, -OH), 12.04 (brs, 1H, -OH); ^{13}C NMR (100 MHz, $CDCl_3$) δ13.9, 14.1, 22.3, 22.6, 25.0, 28.0, 28.2, 29.1, 29.3, 29.4, 31.8, 41.7, 43.4, 65.9, 103.2, 112.7, 116.5, 136.6, 160.3, 164.3, 171.7, 206.7; MS (ESI) m/z 402 ($M+Na^+$, 100%); Analysis calculated for $C_{22}H_{34}O_5$: C, 69.81; H, 9.05. Found: C, 69.65; H, 8.81.

47. Subramanian, A. *et al.* Gene set enrichment analysis: a knowledge-based approach for interpreting genome-wide expression profiles. *Proc. Natl. Acad. Sci. USA* **102**, 15545–15550 (2005).
48. McCoy, A.J. *et al.* Phaser crystallographic software. *J. Appl. Crystallogr.* **40**, 658–674 (2007).
49. Emsley, P., Lohkamp, B., Scott, W.G. & Cowtan, K. Features and development of Coot. *Acta Crystallogr. D Biol. Crystallogr.* **66**, 486–501 (2010).
50. Collaborative Computational Project, Number 4. The CCP4 suite: programs for protein crystallography. *Acta Crystallogr. D Biol. Crystallogr.* **50**, 760–763 (1994).
51. Murshudov, G.N. *et al.* REFMAC5 for the refinement of macromolecular crystal structures. *Acta Crystallogr. D Biol. Crystallogr.* **67**, 355–367 (2011).
52. Murshudov, G.N., Vagin, A.A. & Dodson, E.J. Refinement of macromolecular structures by the maximum-likelihood method. *Acta Crystallogr. D Biol. Crystallogr.* **53**, 240–255 (1997).
53. Cogan, U., Kopelman, M., Mokady, S. & Shinitzky, M. Binding affinities of retinol and related compounds to retinol binding proteins. *Eur. J. Biochem.* **65**, 71–78 (1976).
54. Chen, R., Li, L. & Weng, Z. ZDOCK: an initial-stage protein-docking algorithm. *Proteins* **52**, 80–87 (2003).
55. Li, L., Chen, R. & Weng, Z. RDOCK: refinement of rigid-body protein docking predictions. *Proteins* **53**, 693–707 (2003).
56. Brooks, B.R. *et al.* Charmm—a program for macromolecular energy, minimization, and dynamics calculations. *J. Comput. Chem.* **4**, 187–217 (1983).
57. Banks, J.L. *et al.* Integrated modeling program, applied chemical theory (IMPACT). *J. Comput. Chem.* **26**, 1752–1780 (2005).
58. Shivakumar, D. *et al.* Prediction of absolute solvation free energies using molecular dynamics free energy perturbation and the OPLS force field. *J. Chem. Theory Comput.* **6**, 1509–1519 (2010).

doi:10.1038/nchembio.1788